

## Cr-Doped TiO<sub>2</sub>: Synthesis and Photodegradation of Methylene Blue Dye

M.J. Pawar\*, V.B. Nimbalkar, M.D. Gaonar, A.D. Khajone, S.B. Deshmukh  
Laboratory of Materials Synthesis, Department of Chemistry, Smt. Narsamma ACS College, Kiran Nagar,  
Amravati M.S. India 444606

---

### Abstract

Cr-doped TiO<sub>2</sub> photocatalyst were synthesized successfully by aEDTA-Glycol method. Ethylenediamine was used as a source of N dopantsto extend and improve the photoresponse of the materials to UV light. The photocatalysts werecharacterized by several techniques to determine the structural, textural and optical characteristics. The activity of the materials was tested in the photodegradation of methylene blue (MB) dye. Factors affecting the photodegradation process were studied.

**Keywords:** TiO<sub>2</sub>; Cr-doped TiO<sub>2</sub>; Photocatalysis; N-doped TiO<sub>2</sub>; Methylene Blue Dye;

---

Date of Submission: 20-09-2021

Date of Acceptance: 05-10-2021

---

### I. Introduction

TiO<sub>2</sub> based semiconductor materials have been widely studied for environmental applications due to their efficiency on the degradation and mineralization of organic pollutants in water [1-4]. TiO<sub>2</sub> shows non-toxicity, low cost, chemical stability, resistance to corrosion, and high reactivity under ultraviolet light ( $\lambda < 387$  nm). Recently many researchers have explored different methods to improve visible-light response of TiO<sub>2</sub>, such as dye sensitization, fabrication of a heterojunction with another semiconductor and doping with nonmetal (N, B, F, etc.) and metal elements (Sn, V, Cr, etc.) [5-18]. Among all these, the introduction of metal dopants (especially transition metal) into the TiO<sub>2</sub> lattice is a simple and effective means. As one of the transition metals, Cr has been widely used as the dopant since Cr doping can narrow the band gap and extend the photoresponse to the visible-light range [19–22]. The incorporation of metal dopant ions into the crystal lattice of semiconductor TiO<sub>2</sub> has been widely studied. The transition metal ion dopants expand the light absorption from UV to the visible region, leading to the improvement of the photo-response of TiO<sub>2</sub> by introducing additional energy levels within the band gap of TiO<sub>2</sub> by the dispersion of the metal ions in the TiO<sub>2</sub> matrix [23, 24]. Furthermore, transition metal dopants inhibit electron-hole recombination during irradiation by increasing the charge separation and therefore the efficiency of the photocatalytic process.

Chromium(III) ion (Cr<sup>3+</sup>) has been considered an appropriate dopant candidate, because the similar ionic radius of Cr<sup>3+</sup> (0.63 nm) compared to that of Ti<sup>4+</sup> (0.68 nm) enables the easy incorporation of chromium into the crystal lattice of TiO<sub>2</sub> [25-27]. Moreover, the Cr-doped samples may even exhibit inferior UV-light photocatalytic activity compared to TiO<sub>2</sub>. In fact, the enhancement of the photocatalytic activity under visible light irradiation has been demonstrated by doping TiO<sub>2</sub> with Cr<sup>3+</sup> ion, with the consequent retarding of the recombination process of electron-hole pairs [26].

The material properties of the prepared catalyst seem to be strictly dependent on the crystal structure of the catalyst, the size and morphology of the nanoparticle, which are correlated with the method of synthesis, and the dopant content. Furthermore, the preparation techniques used to synthesize transition metal doped TiO<sub>2</sub> materials play an important role on the photostability of the catalyst because these dopants generally exhibit different oxidation states and therefore redox reactions could take place during the synthesis [27].

On the above grounds Cr<sup>3+</sup>-doped titanium dioxide was prepared by EDTA-Glycol method. The prepared catalyst was characterized by X-ray diffraction (XRD), ultraviolet-visible diffuse reflectance spectroscopy (UV-Vis DRS), N<sub>2</sub> adsorption-desorption analysis, scanning electron microscopy (SEM), transmission electron microscopy (TEM) and photoluminescence (PL) spectroscopy. For photocatalytic evaluation activity, methylene blue indicator (MB) was chosen as a model pollutant. The photocatalytic activity of the Cr<sup>3+</sup>-doped TiO<sub>2</sub> was assessed by degradation of MB aqueous solution under UV light and was subsequently compared with the performances of the pure TiO<sub>2</sub> and Degussa P25. Moreover, the stability and recyclability of the Cr<sup>3+</sup>-doped TiO<sub>2</sub> catalyst for MB degradation was evaluated.

## II. Experimental

### 2.1 Synthesis of Undoped and Cr doped TiO<sub>2</sub>

All chemicals were obtained from the indicated sources and used without further purification. Titanium tetraisopropoxide (TTIP, 98% Sigma Aldrich), Chromium nitrate (98% Sigma Aldrich), Ethylene diamine tetra acetic acid (EDTA, 98% Sigma Aldrich), Iso propanol (99.9% Sigma Aldrich), Ethanol (99.9% Sigma Aldrich) and distilled water (DW).

The solution of Titanium isopropoxide (TTIP) prepared in ethanol-Iso propanol (1:1). To this solution, calculated amount of chromium nitrate (CN) was added to get the materials with the atomic ratio of Cr to Ti in the precursor as 1%, 4% and 7% respectively. To this mixture, different amounts of EDTA and EG were added under the stirring condition. The prepared mixtures were then continuously stirred for 4 h to obtain a gel like material. After 4 h stirring, they were transferred into autoclaves and heated at 200°C for 5 h. The precipitates were rinsed with ethanol and were collected by centrifugal separation. Pure and doped TiO<sub>2</sub> nanomaterials were finally obtained by calcination of the precipitates at 450°C for 2 h at the heating rate of 10°C/min.

**Table 1 Atomic ratio, Crystalline Phase, Lattice parameters and Average Crystallite Size of prepared samples.**

Sample Code	Atomic Ratio of Cr (%)	Crystalline Phase	Crystallite Size (nm)	Lattice Parameters (Å)	
				a = b	c
TiO <sub>2</sub>	0	Anatase	19.8	3.783	9.523
TC-1	1	Anatase	18.9	3.784	9.523
TC-4	4	Anatase	10.8	3.784	9.523
TC-7	7	Anatase	21.6	3.787	9.526

### 2.2 Characterization

Crystallographic phase analysis was carried out from powder X-ray diffraction (XRD) measurements using a Phillips analytical diffractometer with Ni-filtered Cu K $\alpha$  radiation. The average crystallite size of anatase and rutile phases was determined from the Scherrer equation after correcting for the instrumental broadening. TEM (Transmission electron microscope) data were obtained using a 200 kV FEI Tecnai T20 machine. EDS (Energy dispersive X-ray) spectroscopy was used to determine the approximate elemental composition of the samples. BET surface area, pore volume, and pore size distribution profiles were obtained using a Micromeritics ASAP 2020 analyzer. About 100 mg of a sample was degassed under vacuum (10<sup>-6</sup> Torr) at 300°C, prior to N<sub>2</sub> adsorption. The BJH method was employed to obtain the pore size distribution. UV-vis absorption and PL spectra measurements were carried out using portable multichannel optical spectrum analyzer.

### 2.3 Photocatalytic Decolorization of Methylene Blue (MB)

The photocatalytic reactivity of N-doped TiO<sub>2</sub> was evaluated by the decolorization of MB under visible light irradiation (> 400 nm). A LED lamp of 15 W was used as a light source for testing. Different amounts of the Zn-doped TiO<sub>2</sub> powder was added into 20 ml of 5-20 mg/L MB solution. Before open LED light, the suspension was put in the reactor and stirred until dye adsorption was completed. After that, the LED light was turned on. The concentration of MB dye solution was evaluated at given time intervals of every 30 min by using UV-vis spectrophotometry at wavelength of 670 nm ( $\lambda_{max}$ ).

## III. Results And Discussion

### 3.1 X-ray diffraction studies

XRD is the effective means to determine whether or not the Cr ions are doped into TiO<sub>2</sub> crystalline lattice. Figure 1 shows the XRD patterns of Cr-doped and pure TiO<sub>2</sub> samples. All of the synthesized samples can be well indexed to the anatase phase. The peaks at 25.33, 36.89, 37.83, 38.64, 48.99, 53.94, and 55.14 can be ascribed to (101), (103), (004), (112), (200), (105), and (211) planes of anatase, respectively (JCPDF Card No. 65-5714). As no separate phase is detected, the doped Cr ions do not exist in the form of Cr<sub>2</sub>O<sub>3</sub> or other Cr(VI) species. Compared with the undoped TiO<sub>2</sub>, the full width at half maximum (FWHM) of the XRD peaks becomes larger for the doped samples (Figure 1), indicating that introduction of Cr ions can lead to a decrease in the crystallite size of TiO<sub>2</sub>.

The crystallite size can be calculated using the Debye-Scherrer equation –

$$d = \frac{k\lambda}{\beta \cos\theta} \quad (1)$$

where,  $\lambda$  is the wavelength of the X-ray radiation ( $k = 0.15406$  nm),  $k$  is usually taken as 0.89, and  $\beta$  is the line width at half-maximum height of the main intensity peak after subtraction of the equipment broadening.

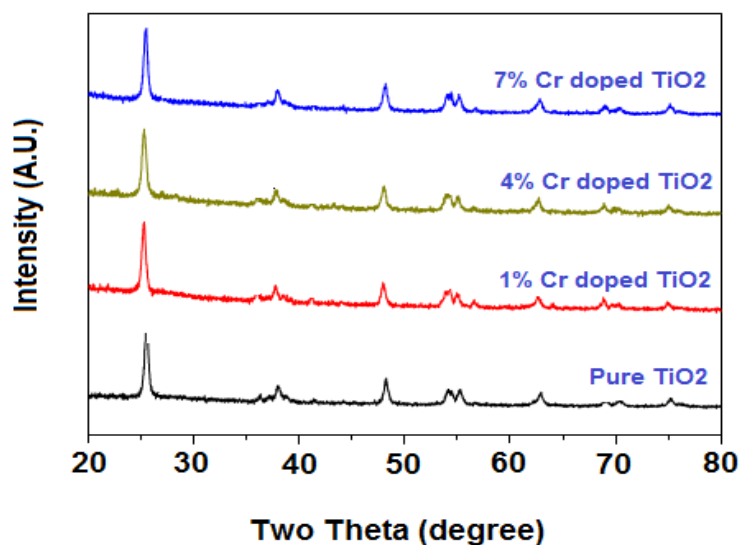


Figure 1 XRD pattern of pure and Cr doped TiO<sub>2</sub>.

### 3.2 TEM analysis

TEM (Figure 2) measurements were carried out to study the surface features of the pure and doped TiO<sub>2</sub> samples. TEM micrographs also demonstrated that the synthesized nanoparticles were homogeneous, with no significant phase separation on the surface. Both, pure and doped TiO<sub>2</sub> samples were composed of large quantity of well-dispersed spherical nanoparticles with uniform size and shape with average size estimated from the TEM image of 19.8 nm and 10.8 nm, respectively. The introduction of chromium into the TiO<sub>2</sub> lattice attenuates agglomeration and grain growth that could improve the photocatalytic performance and the potential application on the removal of wastewater pollutants of the doped catalyst. A similar effect has also been described in Cr<sup>3+</sup>-doped TiO<sub>2</sub> nanoparticles synthesized by a microwave technique [28].

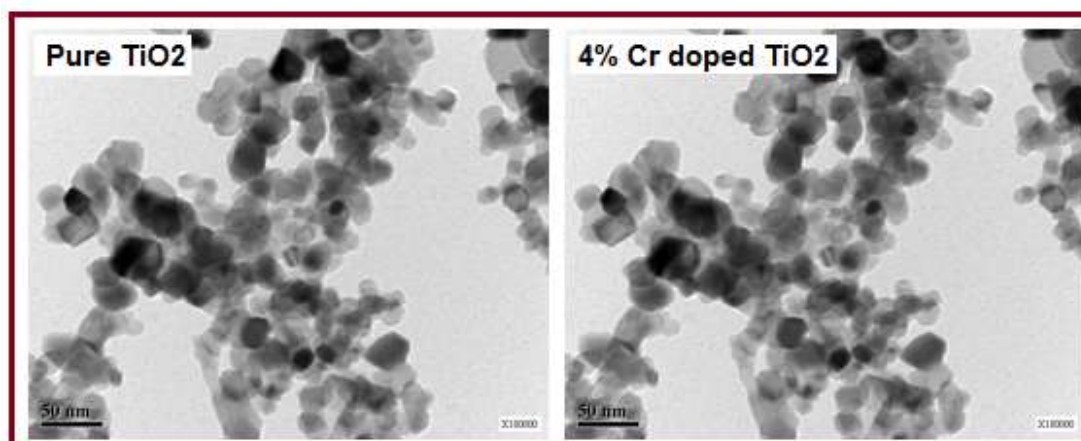


Figure 2. TEM micrographs of pure TiO<sub>2</sub> and 4% Cr doped TiO<sub>2</sub> samples.

### 3.3 Photoluminescence Spectra

PL spectra of pure and Cr doped TiO<sub>2</sub> samples are obtained using xenon flash lamp having excitation wavelength of  $\lambda_{\text{ex}} = 345$  nm as shown in Figure 3. PL spectroscopy gives information related to lattice defects, oxygen vacancies, and charge trapping that can be greatly influenced by ion doping. Thus, PL spectroscopy was used to investigate the Cr (III) doping behaviour in TiO<sub>2</sub>. Two maximum centered at 463 nm and 571 nm were found in samples. No new peaks were observed for the doped sample, indicating that the doping of Cr into TiO<sub>2</sub> lattice did not form new defects related to PL emissions. In agreement with previous studies [29] it was noted the decrease in the emission intensities after Cr doping. Thus, these results confirmed that the doped Cr<sup>3+</sup> ions (3d<sup>2</sup>4s<sup>1</sup>) can capture photogenerated holes to form more stable Cr<sup>4+</sup> or Cr<sup>6+</sup> ions and decrease the recombination

rate of these separated charges [30]. Moreover, the weak UV shoulder at 396 nm and the peaks at 414, 419, and 436 nm in undoped TiO<sub>2</sub> are diminished with the addition of Cr(III) dopant in TiO<sub>2</sub>, which further supports the shifting of the absorption spectra from the UV region to the visible region[29].

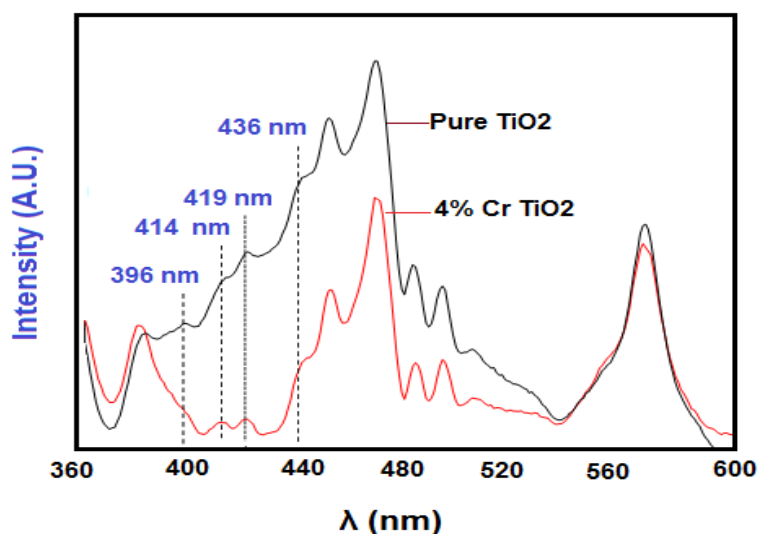


Figure 3. PL spectra of pure and 4% Cr doped TiO<sub>2</sub> at room temperature.

### 3.4 BET Analysis

As shown in Table 2, specific surface area (BET) was higher for Cr doped TiO<sub>2</sub> than for pure TiO<sub>2</sub> sample. Large surface areas are advantageous as allows an increased adsorption of pollutant molecules on the active surface sites. Both samples are mesoporous with an average pore diameter is in the range between 54.7 and 77.4 Å for pure and Cr doped TiO<sub>2</sub> samples.

Table 2 Specific surface area and pore diameter of pure and Cr doped TiO<sub>2</sub> samples.

Sample	Surface Area(m <sup>2</sup> /g)	Pore Diameter(Å)
TiO <sub>2</sub>	52.2	54.7
TC-1	57.6	59.4
TC-4	63.9	77.4
TC-7	53.1	56.7

### 3.5 UV-vis absorption spectra

For the study of the optical properties of synthesized samples, a classic method of UV absorption spectroscopy was applied. All spectra were measured at room temperature in the same geometry and the same experimental conditions, and the results were compared using standard statistical treatment routines. The absorption spectra of pure and Cr-doped TiO<sub>2</sub> samples shown in Figure 4 are quite different both for pure and Cr doped TiO<sub>2</sub>, indicating a significant effect of on the properties of TiO<sub>2</sub> nanocrystallites.

Near the UV absorption edge the absorption peaks are observed for anatase TiO<sub>2</sub> samples at 2.91 eV. This suggests that the UV-absorption peaks can be associated with the existence of defect levels inside the band gap. The calculated energy of the TiO<sub>2</sub> lowest phonon-assisted indirect allowed (IA) transition from the valence band (VB) to the conduction band (CB) is 2.91 eV [38]. We assumed that in our case the UV absorption peak at 2.91 eV can be assigned to overlapping of the lowest-energy fundamental absorption and absorption by Ti<sup>3+</sup> localized states. In the absorption spectra of the studied samples, spectral features at 3.05 and 3.19 eV marked by arrows, are distinguished by changing the slope of the tangent to absorption curve. These features, according to theoretical predictions of Daude et al. [31], can be associated with the fundamental or intrinsic absorption of anatase TiO<sub>2</sub>.

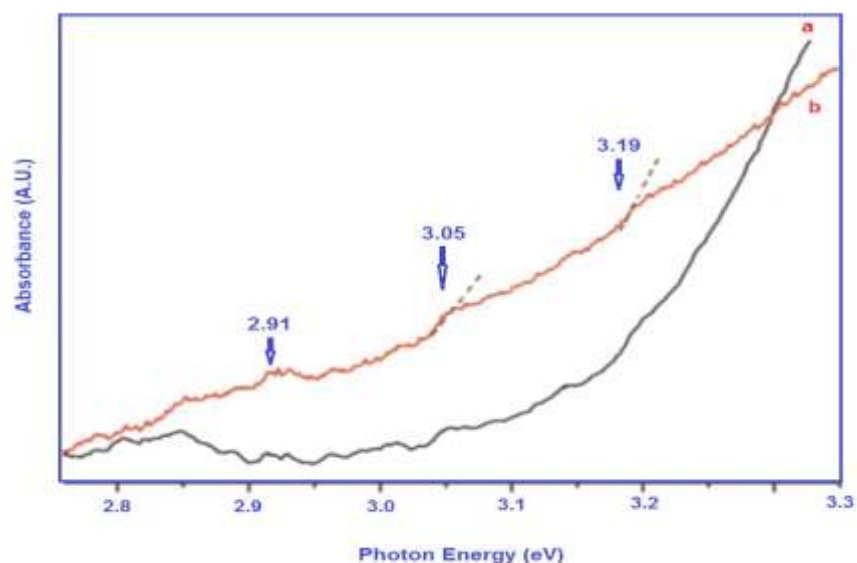


Figure 4. UV-vis absorption spectra of a) pure TiO<sub>2</sub> and 4% Cr-doped TiO<sub>2</sub>.

#### IV. Photocatalytic activity of pure and Cr-doped TiO<sub>2</sub> materials

Photocatalytic activity of synthesized pure samples was determined by investigating the degradation of MB dye under the UV-light and sunlight exposure.

##### 4.1 Effect of Catalyst

The photocatalytic activity of the synthesized samples was evaluated by measuring the photodegradation of MB as a function of irradiation time under UV light. The prepared MB solution was having intense absorption at 664 nm. The MB solution with 0.4 g/L catalyst dose was stirred well and allowed to UV light irradiation at regular intervals and the corresponding absorption spectra were measured.

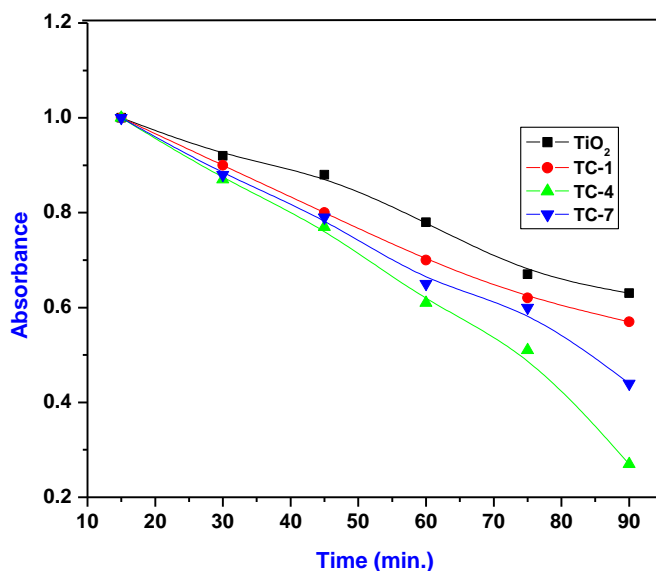


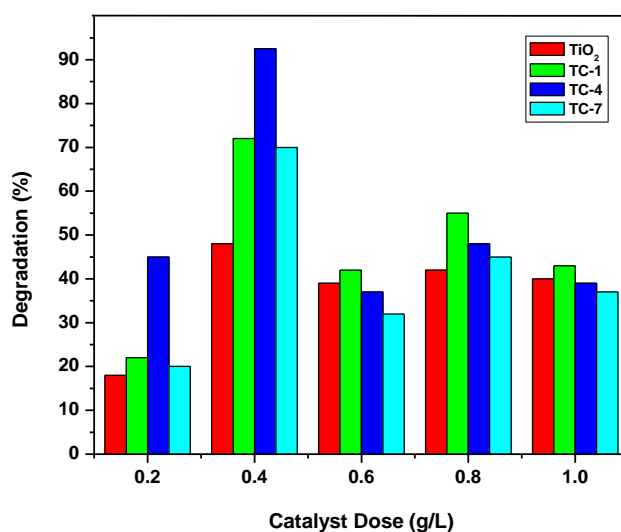
Figure 5. Degradation of MB dye with pure and Cr-doped TiO<sub>2</sub>. ([MB]<sub>0</sub> = 20 mg/L, Catalyst dose = 0.4 g/L, pH=9.5, light intensity = 50.0 mW/cm<sup>2</sup>)

Figure 5 shows the comparative graph for degradation of MB dye with pure and Cr-doped TiO<sub>2</sub> nanoparticles under UV light. The results show that higher the irradiation time, more is the decolorization of dye and lesser is the absorbance. Therefore the study also reveals that the photocatalyst can degrade the dye to maximum extent in 90 min. Photocatalytic activity of Cr-doped TiO<sub>2</sub> sample was found more than pure TiO<sub>2</sub> nanoparticles indicating the modification in the band gap. The high photocatalytic efficiency of the Cr-doped

TiO<sub>2</sub> can be attributed to the reconstructed favorable surface structure with the incorporated Cr–O–Ti bonds and their structure with high surface area, which is able to facilitate adsorption of water contaminants and effective utilization of UV light. With the same calcination temperature, the surface area of Cr-doped TiO<sub>2</sub> was significantly larger than that of the undoped one. The highest photocatalytic activity was observed for anatase TC-4 sample with the largest surface area (63.9 m<sup>2</sup>/g) and pore diameter (77.4 Å).

#### 4.2 Effect of Catalyst load

Figure 6 indicates that the rate of photocatalytic degradation of MB under UV light increases as the dose of catalyst is increased from 0.1 g/L to 1.0 g/L due to the increased surface area and hence greater number of active sites available for adsorption of dye molecules. However, further increase of catalyst concentration results in lower photocatalytic degradation which can be attributed to light scattering caused by the turbidity of the solution.



**Figure 6** Photocatalytic degradation of MB dye as a function of catalyst dose. ([MB]<sub>0</sub> = 20 mg/L, pH=9.5, light intensity = 50.0 mW/cm<sup>2</sup>)

#### 4.3 Effect of the initial dye concentration

Figure 7 shows that the photodegradation of MB dye increases initially as the initial concentration of MB is increased from 10 to 20 mg/L and then goes on decreases as the initial concentration of MB is increased from 20 to 50 mg/L. The lower degradation efficiency at higher initial concentration can be attributed to the fact that the higher MB concentrations could absorb more photons, which reduces the available photons to activate the TiO<sub>2</sub> which results in reduced degradation efficiency [32].

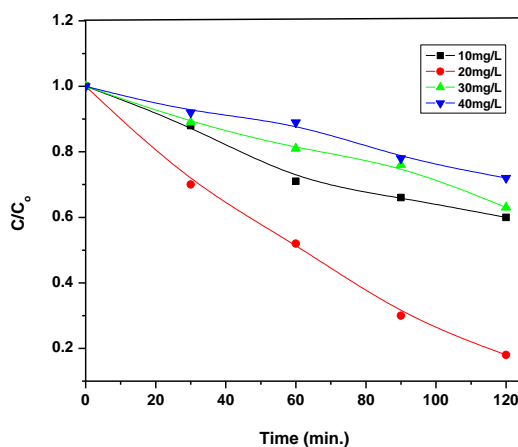


**Figure 7** Effect of initial concentration of MB on the photodegradation of MB dye under UV light. (Catalyst dose = 0.4 g/L, pH = 9.5, light intensity = 50.0 mW/cm<sup>2</sup>)

#### 4.4 Effect of oxygen purging

The effect of air, oxygen and nitrogen bubbling on the degradation of MB dye under UV light is illustrated in Figure 8, where the rate of MB degradation in oxygen bubbling solution is three times higher than that in nitrogen bubbling solution. This implies that oxygen plays a critical role in solar TiO<sub>2</sub>-based photocatalysis, enhancing the degradation efficiency even under lower concentration (20% oxygen in air, i.e. static oxygen).

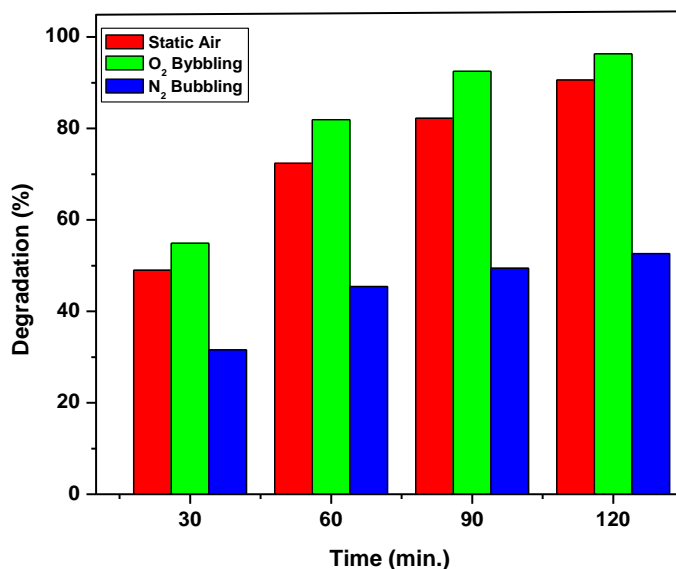


**Figure 8.** Effect of gas purging on the photocatalytic degradation of MB under UV light. ([MB] = 20 mg/L, Catalyst dose = 0.4 g/L, pH = 9.5, light intensity = 50.0 mW/cm<sup>2</sup>).

#### 4.5 Effect of increase in temperature

The effect of increasing temperature was observed on the photodegradation of MB dye for the sample TC-4 and Degussa P25 by varying the temperature from 298 to 328 K, keeping the dye concentration constant at 20 mg/L with a catalyst concentration of 0.4 g/L. The results are graphically evaluated by Arrhenius based temperature dependence of the photocatalytic degradation by a plot of  $\log(C_0/C)$  versus  $1/T$  (Figure 9). One can see that, for TC-4 and Degussa P25, the rate of MB degradation increases but recorded as a higher for synthesized sample TC-4. Here we, assumed that, doping with Cr is significant for enhancement of photocatalytic activity of TiO<sub>2</sub>.

It can be seen that with increasing temperature, the rate of the reaction increases which is due to the reason that increase in temperature helps to speed-up the velocity of both the hydroxyl radicals and the dye molecules to interact with each other thus the reaction competes more efficiently with the electron-hole recombination.

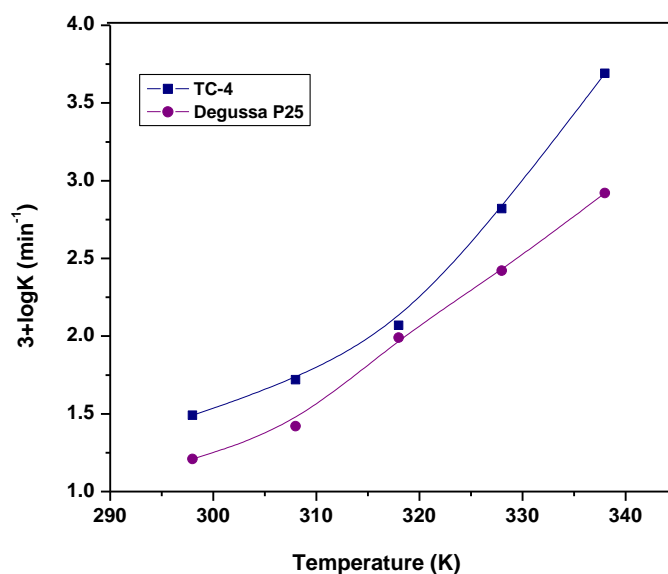


Figure 9. Effect of temperature on the photodegradation of MB dye over sample TC-4 and Degussa P25.

## V. Conclusion

In summary, doping Cr in TiO<sub>2</sub> was successfully carried out by EDTA-Glycol method. XRD pattern suggests that TiO<sub>2</sub> is not changed its structure by Cr doping. The optimized condition for the best photoresponse of TiO<sub>2</sub> in visible light is obtained by doping with the atomic ratio of Cr to Ti as 4%. The photocatalytic degradation of MB solution by Cr-doped TiO<sub>2</sub> photocatalysts was experimentally investigated by using UV-vis spectrophotometry. From kinetic studies it was found that the method of photodegradation is dependent on parameters such as catalyst loadings, initial dye concentration, oxygen purging and temperature. TiO<sub>2</sub> itself shows less degradation rate than Cr-doped TiO<sub>2</sub> when the irradiation time is up to 90 min. These results imply that doping Cr in TiO<sub>2</sub> can improve the photocatalytic activity due to narrowed band gap energy can be scaled-up for enhancement of photocatalytic degradation under UV light for industrial applications.

## References

- [1]. Daghrir R, Drogui P, Robert D. *Industrial and Engineering Chemistry Research*, 2013; (52):3581- 3599.
- [2]. Pelaez M, Nolan N.T, Pillai S.C, Seery M.K, Falaras P, Kontos A.G, Dunlop P.S.M, Hamilton J.W.J, Byrne J.A, O'Shea K, Entezari MH, Dionysiou D.D. *Applied Catalysis B: Environmental*, 2012;(125):331-349.
- [3]. Wang R, Jiang G, Ding Y, Wang Y, Sun X, Wang X, Chen W. *ACS applied materials & interfaces*, 2011;(3):4154-4158.
- [4]. Jiang G, Wang X, Zhou Y, Wang R, Hu R, Xi X, Chen W. *Materials Letters*, 2012;(89):59-62.
- [5]. Zhao, J.C, Wu, T.X, Wu, K.Q, Oikawa, K, Hidaka, H, Serpone, N. *Environ. Sci. Technol.*, 1998;(32):2394-2400.
- [6]. Yin, M. C, Li, Z. S, Kou, J. H, Zou, Z. G. *Environ. Sci. Technol.*, 2009;(43):8361-8366.
- [7]. Fung, A. K. M, Chiu, B. K. W, Lam, M. H. W. *Water Res.*, 2003;(37):1939-1947.
- [8]. Hattori, A, Yokihisa, Y, Tada, H, Ito, S. *J. Electrochem. Soc.*, 2000;(147):2279-2283.
- [9]. Wu, C.H. *Chemosphere*, 2004; (57): 601-608.
- [10]. Kim, Y.J, Gao, B, Han, S.Y, Jung, M.H, Chakraborty, A.K, Ko, T, Lee, C, Lee, W. I. *J. Phys. Chem. C*, 2009;(113):19179-19184.
- [11]. Asahi, R, Morikawa, T, Ohwaki, T, Aoki, K, Taga, Y. *Science*, 2001;(293): 269-271.
- [12]. Livraghi, S, Paganini, M.C, Giamello, E, Selloni, A, Di Valentin, C, Pacchioni, G. *J. Am. Chem. Soc.*, 2006;(128):15666-15671.
- [13]. Zhao, W, Ma, W.H, Chen, C.C, Zhao, J.C, Shuai, Z.G. *J. Am. Chem. Soc.*, 2004;(126):4782-4783.
- [14]. Yu, J. C, Yu, J. G, Ho, W. K, Jiang, Z.T, Zhang, L.Z. *Chem. Mater.*, 2002;(14):3808-3816.
- [15]. Wang, W. L, Shang, Q.K, Zheng, W, Yu, H, Feng, X.J, Wang, Z.D, Zhang, Y.B, Li, G.Q. *J. Phys. Chem. C*, 2010;(114):13663-13645.
- [16]. Sakatani, Y, Ando, H, Okusako, K, Koike, H, Nunoshige, J, Takata, T, Kondo, J.N, Hara, M, Domen, K. *J. Mater. Res.*, 2004;(19): 2100-2108.
- [17]. Klosek, S, Raftery, D. *J. Phys. Chem. B*, 2001;(105): 2815-2819.
- [18]. Shi, J.Y, Leng, W.H, Zhu, W.C, Zhang, J.Q, Cao, C.N. *Chem. Eng. Technol.*, 2006;(29):146-.
- [19]. Pan, L, Zou, J. J, Zhang X. W, Wang, L. *Ind. Eng. Chem. Res.*, 2010;(49): 8526-.
- [20]. Murakami, N, Chiyoya, T, Tsubota, T, Ohno, T. *Appl. Catal., A*, 2008;(348): 148-.
- [21]. Buddee, S, Wongnawa, S, Sirimahachai, U, Puetpaibool, W. *Mater. Chem. Phys.*, 2011;(126):167-.
- [22]. Jaimy K.B, Ghosh S, Sankar S, Warriar K.G.K. *Materials Research Bulletin*, 2011;(46):914-21.
- [23]. Ould-Chikh S, Proux O, Afanasiev P, Khrouz L, Hedhili M.N, Anjum D.H, Harb M, Geantet C, Basset J.M, Puzenat E. *Chem. Sus. Chem.* 2014;(7):1361-1371.
- [24]. Fan X, Chen X, Zhu S, Li Z, Yu T, Ye J, Zou Z. *Journal of Molecular Catalysis A: Chemical*, 2008;(284):155-160.
- [25]. Tian B, Li C, Zhang J. *Chemical Engineering Journal*, 2012;(191):402-409.
- [26]. Pedraza-Avella J.A, López R, Martínez-Ortega F, Páez-Mozo E.A, Gómez R. *Journal of Nano Research*, 2009;(5):95-104.



- [27]. Vijayalakshmi K, Jereil S.D. *Journal of Materials Science: Materials in Electronics*, 2015;(26):3790-3796.  
[28]. Khan H, Swati I.K. *Industrial & Engineering Chemistry Research*, 2016;(55):6619-6133.  
[29]. Li X, Guo Z, He T. *Physical Chemistry Chemical Physics*, 2013;(15):20037- 20045.  
[30]. Daude,N. Gout, C.Jouanin, C.*Phys. Rev. B*,1977; (15):3229-3236.  
[31]. Mumiandy,S.S. Kaus,N.H.M. Jiang,Z.-T. Altarawneh, M. Lee,H.L. *RSC Adv*, 2017;(7):48083–48094.

M.J. Pawar, et. al. " Cr-Doped TiO<sub>2</sub>: Synthesis and Photodegradation of Methylene Blue Dye." *IOSR Journal of Applied Chemistry (IOSR-JAC)* 14(09), (2021): 54-62.